American Mineralogist, Volume 81, pages 1195–1207, 1996

Trace element zoning in pelitic garnet of the Black Hills, South Dakota

CRAIG S. SCHWANDT,[1] JAMES J. PAPIKE,[2] AND CHARLES K. SHEARER[2]

[1]NASA, Johnson Space Center, SN4, Houston, Texas 77058, U.S.A.
[2]Institute of Meteoritics, Department of Earth and Planetary Sciences, University of New Mexico, Albuquerque, New Mexico 87131, U.S.A.

ABSTRACT

Trace element (REE, Cr, Ti, V, Y, and Zr) analysis of garnet from the garnet, staurolite, and lower sillimanite zones of an aluminous schist of the Black Hills, South Dakota, indicates that REE zoning varies as a function of grade. Garnet-zone garnet has high concentrations of REEs, Cr, Ti, V, Y, and Zr in the cores and low concentrations in the rims. Profiles of heavy REEs contain inflections between the cores and rims, which are approximately symmetric about the cores. Staurolite-zone garnet contains cores enriched with Y and heavy REEs, which decrease toward the rim and increase again at the rim edges but to lower concentrations than in the cores. Cr, V, Ti, Zr, and light REE zoning is less pronounced than heavy REE zoning and is less symmetric about the garnet cores. Almandine-rich garnet of the lower sillimanite zone displays no major element zonation. Trace element (Ti, Cr, V, and Zr) concentrations are minimal, and the zoning is irregular and not symmetric about the garnet cores. Garnet from all three zones has core-to-rim Fe/(Fe + Mg) profiles that suggest garnet growth was uninterrupted with respect to major element components and that Mn zoning formed by a fractionation process. Analysis of trace element zoning in this garnet reveals that the major element zoning was relatively unaffected by volume-diffusion reequilibration. Trace element zonation of all samples of garnet is best explained by a fractionation mechanism in conjunction with limited intergranular diffusion and changing partition coefficients during garnet growth. Heavy REE partitioning is especially dependent on the major element composition of garnet. This research complements previous research by others on the use of trace elements as metamorphic petrogenetic indicators, which demonstrated the importance of bulk-rock composition and phase assemblage on trace element partitioning.

INTRODUCTION

In the past decade great advances have been made in understanding metamorphic phase equilibria and pressure-temperature-time paths (e.g., Spear 1993). These advances primarily use major element compositions of metamorphic minerals. Only limited use is made of the trace element compositions of metamorphic minerals (Hickmott and Spear 1992), although trace element information has, for some time, been an invaluable tool for deciphering igneous petrogenetic paths. Recent advances in analytical geochemistry, such as secondary ion mass spectrometry and laser-ablation mass spectrometry, provide the sensitivity and spatial resolution required for determination of the trace element chemistry of metamorphic minerals, many of which have compositional zoning and, thereby, preserve petrogenetic information.

Recent research (e.g., Erambert and Austrheim 1993; Jamtveit and Hervig 1994) suggests that metamorphic fluids and deformation may influence major element zoning in garnet more strongly than previously assumed. Investigation of trace element zoning in minerals could help elucidate petrogenetic processes because the partitioning of incompatible trace elements is more sensitive to changes in temperature, pressure, and composition than the partitioning of compatible major elements (e.g., McKay 1989; Hickmott and Spear 1992). Investigations using microbeam techniques have revealed that metamorphic minerals contain trace element and O-isotope zonation, which provides valuable petrogenetic "path" information previously unobtainable using only major element techniques (Hickmott et al. 1987; Hickmott and Shimizu 1990; Schwandt 1991; Hickmott and Spear 1992; Schwandt et al. 1993; Kohn et al. 1993; Young and Rumble 1993; Chamberlain and Conrad 1993).

Rare earth elements are especially useful petrogenetic indicators because they are chemically similar but vary systematically in cationic size (Goldschmidt 1937; McKay 1989). Igneous mineral-melt element partition coefficients, the measure of an element's compatibility in a mineral, are dependent on temperature, pressure, and composition (Banno and Matsui 1973; Drake and Weill 1975; Navrotsky 1978; Ford et al. 1983; Colson et al. 1988; McKay 1989). When modeling the trace element

0003–004X/96/0910–1195$05.00

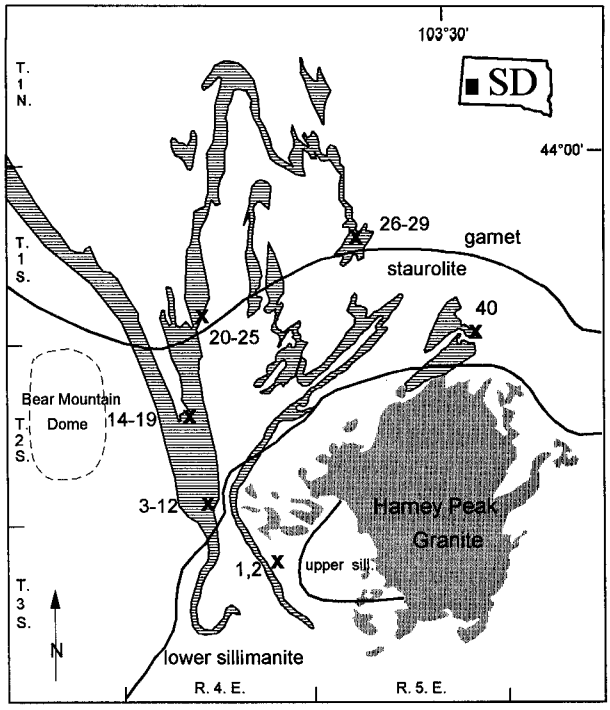

FIGURE 1. Partial geologic map of the southern Black Hills, South Dakota (DeWitt et al. 1989). Ruled pattern represents the Proterozoic metamorphosed tuffaceous shale (XMS), the gray pattern represents the Harney Peak Granite. Solid lines mark isograds.

signatures of melts, trace element partitioning is governed by bulk distribution coefficients, which are functions of the minerals in the model mantle and their proportions (Hanson 1978). In a metamorphic system, the partitioning is between solids or between solids and fluid. Therefore the garnet-matrix bulk distribution coefficient for a trace element is a function of the other matrix phases and their proportions relative to garnet. Hence, the investigation of trace element zoning in metamorphic minerals should expound on the processes occurring during metamorphism.

Excellent exposures of igneous and metamorphic rocks in the southern Black Hills of South Dakota provide a unique natural laboratory for exploring Proterozoic orogeny. Our study utilized a compositionally homogeneous amphibolite-grade pelitic schist (Redden 1968; Redden et al. 1982; Schwandt 1991) of the Black Hills, South Dakota. The schist is transected by two major isograds typical of pelitic schists (e.g., Helms and Labotka 1991). These attributes help simplify interpretation of the trace element zoning in minerals like garnet by minimizing the effects of bulk composition. Garnet from the schist was examined by electron microprobe (EMP) to obtain major element information and by secondary ion mass spectrometry (SIMS) using an ion microprobe to obtain trace element information. SIMS analyses are limited to garnet because of the lack of appropriate standards for the other minerals in the assemblage. However, garnet is useful because it is a relatively refractory mineral that can grow over a rather wide range of temperature and pressure conditions. Therefore, the trace element zonation observed in garnet samples from the three metamorphic zones formed from the same bulk composition identify the most important processes that occurred during garnet growth. The data provide further groundwork for the utilization of trace elements as petrogenetic indicators in metamorphic rock suites.

GEOLOGIC AND PETROLOGIC BACKGROUND

The petrogenetic history of the southern Black Hills (Fig. 1) predominantly records low-pressure, high-temperature metamorphism accompanying emplacement of the Harney Peak Granite (HPG) and associated pegmatites (Redden 1963, 1968; Ratte and Wayland 1969; Redden and Norton 1975; Ratte 1986; Redden et al. 1982, 1990; Terry and Friberg 1990; Schwandt 1991; Helms and Labotka 1991). The core of the southern Black Hills consists of a thick stratigraphic sequence of Proterozoic metasedimentary and metavolcanic phyllites and schists surrounding the 1.7 Ga Harney Peak Granite (e.g., Riley 1970; Walker et al. 1986). A minimum of three periods of deformation and at least two phases of metamorphism have been identified (Redden et al. 1982, 1990). The first deformation folded a stratigraphic sequence of turbidites and volcanic rocks into east-northeast–trending, northerly directed nappes and thrusts. The second deformation refolded the nappes into steep south plunging isoclinal folds that trend north to northwest. The peak of regional metamorphism coincided with this second phase of deformation (Helms and Labotka 1991). In addition, uplift of the metasediments and metavolcanic rocks accompanied emplacement of the HPG, a composite batholith of hundreds of smaller granitic intrusions and pegmatites (e.g., Duke et al. 1988; Shearer et al. 1992). A thermal metamorphic event with associated alkali and boron metasomatism accompanied HPG emplacement and variably overprints the thermal metamorphic features (Redden et al. 1990, and personal communication). The core of the Black Hills contains about 24000 pegmatites surrounding the HPG, some of which are enriched with Li, Be, Ba, Rb, Cs, Sn, Ta, Nb, REEs (rare earth elements), or B (e.g., Norton and Redden 1990; Shearer et al. 1992).

Helms and Labotka's (1991) investigation of pelitic schists in the Black Hills concentrated on those located to the west and north of the HPG dome. Rock samples in this study were collected from many of the same sample localities. However, the present study focuses only on garnet from an aluminous Proterozoic schist mapped and named by DeWitt et al. (1989) as the metamorphosed tuffaceous shale (XMS). Estimates of the temperature and pressure conditions during metamorphism were determined with garnet-rim and matrix-mineral compositions and are similar to those calculated by Helms and Labotka (1991). Temperatures using the Ferry and Spear (1978) equation range from 500 to 600 °C, and pressures deter-

mined using the garnet + plagioclase + Al_2SiO_5 + quartz geobarometer of Newton and Haselton (1981) on appropriate samples range from 6 to 3 kbar. Temperatures and pressures cannot be correlated with the zoning profiles because the garnet grains contain only quartz inclusions, and such T and P estimates would rely only on the garnet composition and the poor assumption that the matrix minerals were abundant enough to suffer no compositional changes.

Analytical methods

Major element mineral chemistry

Major element compositions of garnet were determined by wavelength-dispersive X-ray analysis using a JEOL 733 Superprobe. Analytical conditions included an accelerating potential of 15 kV and a beam current of 20 nA, focused to 2 μm in diameter. Counting times were 20 s or less for major elements and 40 s or less for minor elements. Shorter count times occurred if standard deviations of the counts were $\leq 1\%$ before completion of the set time periods. Elemental peaks were calibrated and standardized using silicate minerals as standards. Wavelength-dispersive spectrometry (WDS) data were reduced with Sandia TASK version 8C with Bence and Albee (1968) correction procedures.

The largest garnet grains in thin sections of each sample have diameters approximately equal to the largest garnet diameters observed in hand samples (0.1–1.5 mm). It is therefore concluded that these grains are cut nearly through their centers. Mutually perpendicular EMP traverses were performed. Recent digital X-ray maps (Fig. 2) of a representative garnet confirm that the major element zoning matches that observed with the mutually perpendicular EMP traverses and defines the spatial character of the major element zoning. Additional EMP traverses were conducted immediately adjacent to the ion microprobe craters after SIMS analysis. These analyses, which are presented in this paper, provide major element data for spots nearly identical to those used in the trace element analysis. The major element zonation observed with these traverses (Appendix Table 1) matches the zonation observed with the mutually perpendicular EMP traverses for each garnet prior to SIMS analysis.

Trace element mineral chemistry

Trace element data for selected garnet samples were obtained with a Cameca IMS 3F ion microprobe and collected in sets, on the basis of atomic mass, with the use of the analytical technique of Shimizu and Hart (1982). The first set of data measured the concentrations of the rare earth elements: La, Ce, Nd, Sm, Eu, Dy, Er, and Yb. Set two measured the transition metals: Ti, V, Cr, Y, and Zr. This extensive list of elements covers possible substitutions in the eightfold-coordinated and sixfold-coordinated sites in garnet (e.g., Hickmott and Shimizu 1990). Analysis spots along each ion microprobe traverse were spaced from 30 to ≥ 100 μm apart because of time limitations, the 25–30 μm diameter of the primary ion beam, and the need to avoid inclusions.

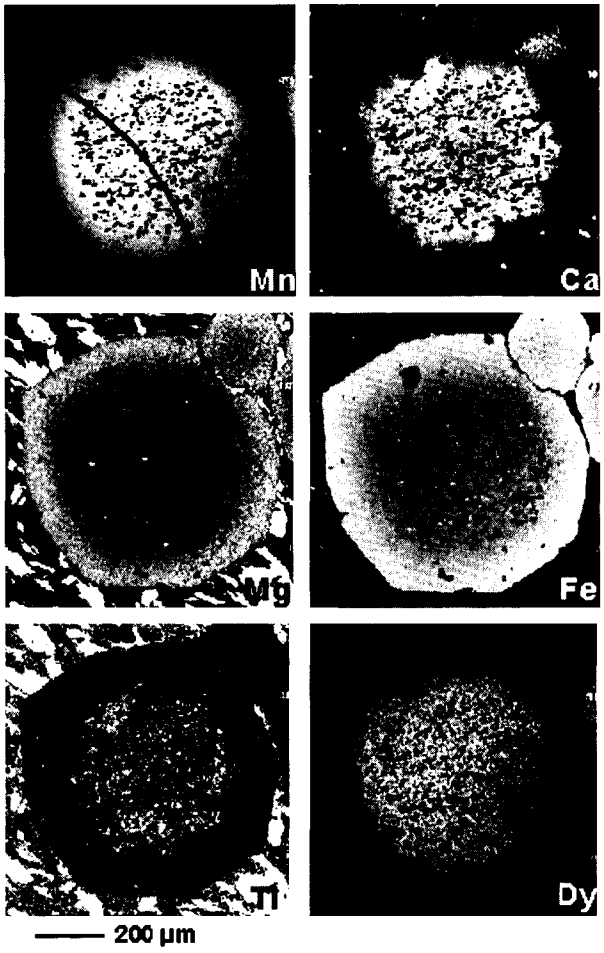

FIGURE 2. Digital elemental X-ray maps of GZ garnet (sample 23). WDS maps demonstrate the concentric zonation of Mn, Ca, Mg, Fe, Ti, and Dy. Ti zoning is irregular. White corresponds to high elemental concentration and black corresponds to low elemental concentration. The black arrow in the Mn map shows the path of the SIMS traverse.

The ion microprobe analyses utilized an O^- primary beam. The trace element isotope intensities were normalized to the Si intensities and converted to part-per-million concentrations with the use of trace element vs. Si working curves determined for a well-characterized pyrope standard for all trace elements. It is difficult to find minerals homogeneous enough to make good SIMS standards. Fortunately, matrix effects on secondary ionization are minimal (e.g., Shimizu and Hart 1982). However, because the garnets of this study are spessartine and almandine-rich, the accuracy of the absolute concentrations may have been affected, but the observed zoning was relatively accurate. It is the relative zoning characteristics, and not the absolute abundances, that are important for the identification of petrogenetic processes (Hickmott and Shimizu 1990). Some of the high trace

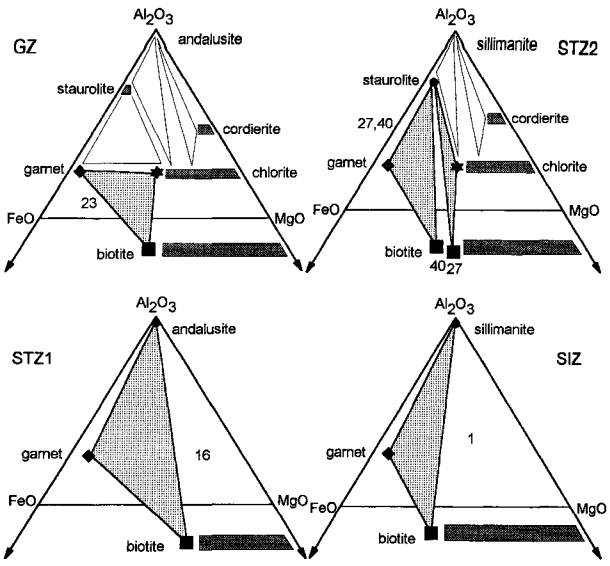

FIGURE 3. AFM projections of the mineral assemblages from each metamorphic zone in the XMS unit. Symbols represent projections of minerals present in each assemblage. Stippled areas denote coexisting phases.

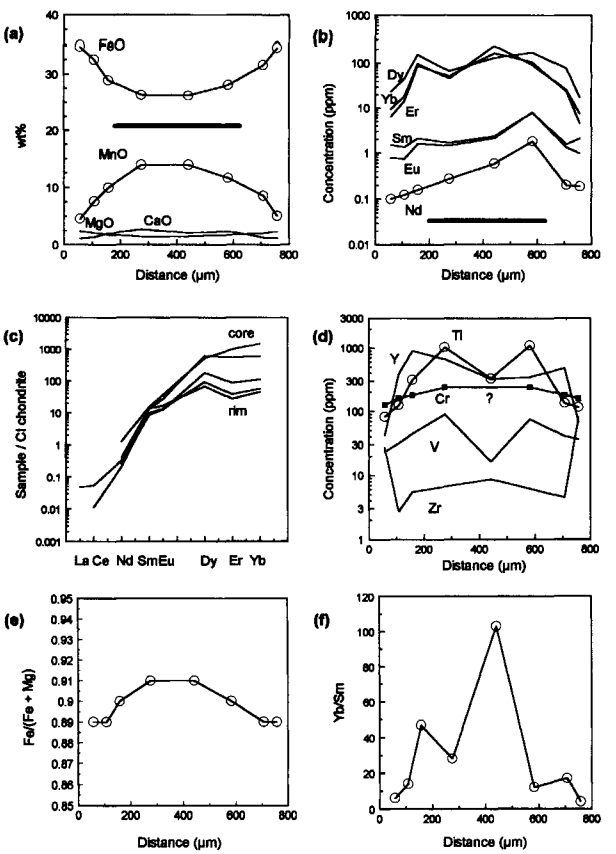

FIGURE 4. Rim-to-rim elemental zonation of a representative GZ garnet (sample 23). Open circles mark positions of SIMS analyses and are the same for each element. Thick lines show inclusion-rich region of crystal. (a) Major element zonation profile determined by EMP at the same positions as the SIMS analyses. (b) REE zonation profile. (c) Chondrite-normalized REE plot of individual SIMS analysis points. (d) Transition element zonation profile. (e) Fe/(Fe + Mg) profile. (f) HREE/LREE profile.

element concentrations were confirmed by WDS mapping analysis with the use of a Cameca SX-100 electron microprobe (Fig. 2). La and Ce measurements typically had unacceptable precision, as concentrations were at or below the detection limits. The accuracy of this SIMS technique is typically within 15%, and precision is within 10% (Shimizu and Hart 1982).

Analysis spots with high Si counts, presumably indicating the incorporation of an inclusion, were eliminated from the traverse data sets. Other analysis spots were eliminated from the data sets, where optical or scanning electron microscopy evidence suggested contamination resulting from crater overlap of inclusions. The major and trace element compositions of representative garnet samples from a slightly larger data set are presented in the following figures and are tabulated in Appendix Table 1.

GARNET OF THE METAMORPHIC ZONES

Garnet is a constituent of the mineral assemblages in the lower sillimanite, staurolite, and garnet zones of the XMS unit (Figs. 1 and 3; Redden et al. 1982, 1990; Helms and Labotka 1991; Schwandt 1991). Garnets in all three zone assemblages lack obvious reaction textures.

Garnet zone

The mineral assemblage of the garnet zone (GZ) consists of garnet + biotite + muscovite + quartz + plagioclase ± chlorite + accessory minerals (Fig. 3). Accessory minerals, which are the same for all three zones, are ilmenite, tourmaline, monazite, and zircon. Garnet samples 23 and 27 are euhedral, 0.8–1.0 mm in diameter, and have cores that are densely packed with quartz inclusions with no preferred orientation. Garnet grains have inclusion-free rims, about 125 μm thick (Fig. 2; Schwandt 1991; Terry and Friberg 1990). Monazite and ilmenite occur rarely as inclusions. No other matrix minerals occur as inclusions. The grains are mildly clustered within the submillimeter grain-sized matrix, with several millimeters between clusters. Chlorite in these samples occurs as variolitic sprays that are in contact with garnet and biotite. The Mn content of this variolitic chlorite is approximately 0.1 wt%.

EMP traverses of the garnet grains revealed symmetric Mn and Fe zoning (Figs. 2, 4a, and 5a). No discontinuity in the compositional zoning occurs at the boundary between the inclusion-rich cores to the inclusion-absent rims. Mn zoning (Figs. 4a and 5a) of the garnet is similar to the classic bell-shaped pattern considered to occur because of a fractionation-depletion mechanism during garnet growth (e.g., Hollister 1966; Tracy et al. 1976; Tracy 1982).

Trace element concentrations of the garnet are higher in the cores than in the rims; even though this zoning is somewhat bell shaped, it does not parallel the bell-shaped major element zoning (Figs. 4 and 5). Trace elements with similar physical and chemical characteristics have similar zonation profiles. HREEs (heavy rare earth elements Dy, Er, Yb) have roughly parallel zonation profiles; Nd, Sm, and Eu, considered as light rare earth elements (LREEs) in addition to La and Ce, also have parallel zonation profiles, but their profiles differ from the HREE profiles (Fig. 5b). HREE/LREE ratios (Figs. 4f and 5f) vary from 10 to 100, with the highest ratios in the cores and intermediate regions of the grains. Near the edges of the inclusion-rich centers, HREE concentrations decrease rimward but then increase in the intermediate portions of the inclusion-free rims (Fig. 5b). HREE concentrations in the cores are more than a factor of ten times higher than the rim concentrations (Figs. 4b and 5b). Ti and V concentrations are about 100 times higher in the cores than at the rims (Fig. 5d). Cr and V zonations approximately parallel each other, with moderate enrichment in the cores relative to the rims. Zr zoning varies among samples (cf. Fig. 4d and 5d).

Chondrite-normalized REE plots for each analysis spot of the trace element traverses display very depleted LREE signatures throughout the garnet. Though the LREE signatures are nearly the same, the HREE signatures are variable. Garnet rim signatures have chondrite-normalized HREE values that are smaller by more than a factor of ten relative to those of the core signatures (Figs. 4c and 5c).

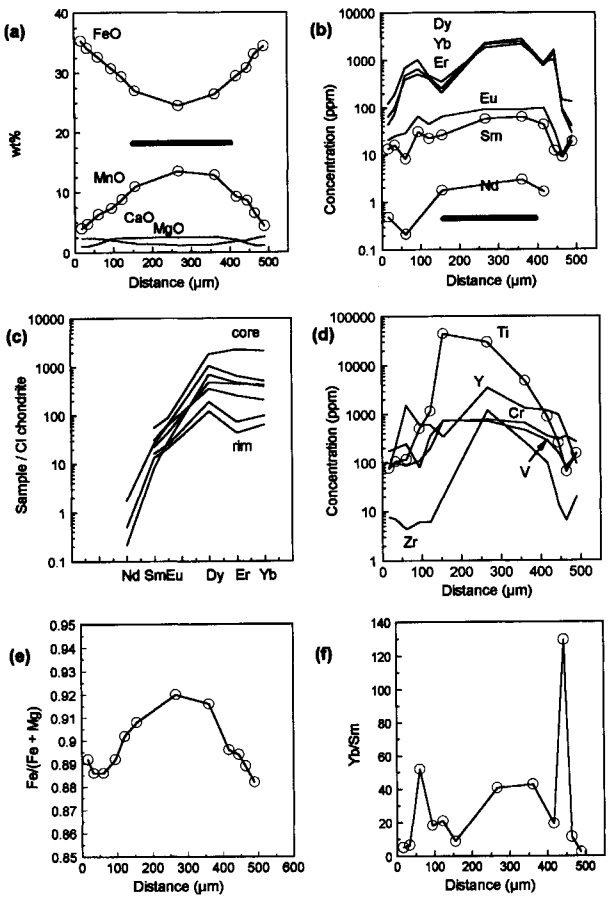

FIGURE 5. Representative rim-to-rim elemental zonation of GZ garnet (sample 27). Open circles mark positions of SIMS analyses and are the same for each element. Thick lines show inclusion-rich region of crystal. (a) Major element zonation profile determined by EMP at the same positions as the SIMS analyses. (b) REE zonation profile. (c) Chondrite-normalized REE plot of individual SIMS analysis points. (d) Transition element zonation profile. (e) Fe/(Fe + Mg) profile. (f) HREE/LREE profile.

Staurolite zone

The staurolite zone (STZ) is represented by two assemblages that differ primarily in the bulk Fe/Mg ratio. The STZ1 assemblage includes the assemblage garnet + biotite + muscovite + chlorite + plagioclase + quartz ± cordierite ± andalusite ± staurolite + accessory minerals. Garnet grains in the southern portion of the STZ1 assemblage are 40–100 μm in diameter, euhedral, and contain a small number of quartz inclusions. These grains are isolated from each other, evenly dispersed throughout the matrix, and have minor Mn zoning with variable rim concentrations. Closer to the staurolite isograd, STZ1 garnet grains are euhedral and larger (800 μm). The STZ1 garnet grains closest to the staurolite isograd have quartz inclusion-rich cores and inclusion-free rims (50–75 μm thick). Mn zoning of STZ1 garnet grains is similar to the Mn zoning of the GZ grains but is much less pronounced (Fig. 6a). The STZ1 garnets are also surrounded by biotite porphyroblasts with no reaction textures, whereas the STZ1 garnet grains farther from the garnet zone reside in the matrix not surrounded by biotite and within smaller biotite porphyroblasts. Minor variolitic chlorite sprays occur in an unoriented fashion relative to the dominant foliation.

The STZ2 assemblage to the north of the HPG (sample 40), contains garnet that is up to 1.5 mm in diameter, subhedral to euhedral, with monazite inclusions. STZ2 garnet has a few weight percent MnO and lacks zoning (Fig. 7a). No reaction textures are apparent at garnet-staurolite contacts. Ellipsoidal concentrations of biotite surrounding quartz cores, 3–4 mm in length, occur in the matrix as apparent pseudomorphs of previous porphyroblasts.

Garnet in the andalusite-bearing mineral assemblage STZ1, west of the HPG, contains bell-shaped Y and HREE zonation, though the concentrations drop to minimal abundances about 100 μm from the rims and then increase toward the rims (Fig. 6b). Ti, V, and Cr zonation is absent, though the elemental abundances decrease in the outer 100 μm of the garnet rims. The STZ2 garnet, from north of the HPG where staurolite occurs in the assemblage, has HREE zonation that is bell shaped (Fig. 7b) but with abundances that are more than a factor of

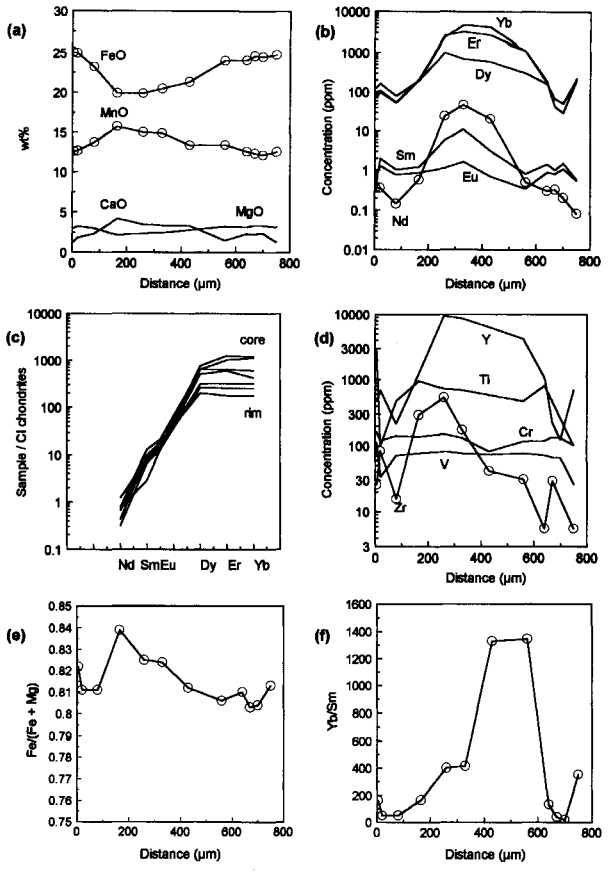

FIGURE 6. Rim-to-rim elemental zonation of staurolite-zone 1 (STZ1) garnet (sample 16). Open circles mark positions of SIMS analyses and are the same for each element. (a) Major element zonation profile determined by EMP at the same positions as the SIMS analyses. (b) REE zonation profile. (c) Chondrite-normalized REE plot of individual SIMS analysis points. (d) Transition element zonation profile. (e) Fe/(Fe + Mg) profile. (f) HREE/LREE profile.

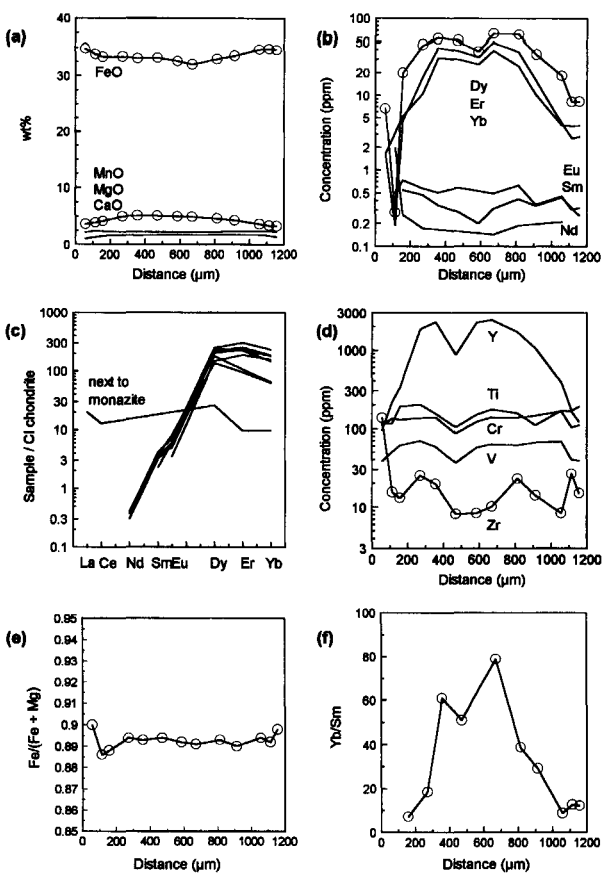

FIGURE 7. Rim-to-rim elemental zonation of staurolite-zone 2 (STZ2) garnet (sample 40). Open circles mark positions of SIMS analyses and are the same for each element. (a) Major element zonation profile determined by EMP at the same positions as the SIMS analyses. (b) REE zonation profile. (c) Chondrite-normalized REE plot of individual SIMS analysis points. (d) Transition element zonation profile. (e) Fe/(Fe + Mg) profile. (f) HREE/LREE profile.

ten smaller than the abundances in the STZ1 garnet. The HREE/LREE within individual STZ2 garnet grains ranges from about six at the rims to about 80 in the cores. The variation in HREE/LREE (Fig. 7f) also shows up on chondrite-normalized plots as the variation in the HREE signatures (Fig. 7c). LREE, Ti, V, Cr, and Zr zonation is absent in STZ2 garnet (Fig. 7), but LREEs, Y, and Zr are slightly enriched in the cores of STZ1 garnet grains (Fig. 6).

Lower sillimanite zone

Garnet + biotite + sillimanite (fibrolite) + muscovite + quartz + plagioclase + accessory minerals make up the lower sillimanite zone (SIZ; sample 1). The subhedral garnet grains are 1–1.5 mm in diameter and contain dispersed inclusions of quartz. SIZ garnet is distinctly Fe-rich with low Mn content and no major element zoning (Fig. 8a). The modal percentage of garnet is low, and the crystals are isolated and randomly distributed in the matrix.

Trace element zonation is minimal (Figs. 8b and 8d). Zonation profiles for REEs, Y, Cr, and V are flat in comparison with the lower grade assemblages; however, the profiles are also asymmetric. In addition, Ti and Zr zonation profiles are variable and not systematic, as they are at lower grades, and abundances are higher on one side of the cores (Fig. 8d). HREE/LREE (Fig. 8f) has an asymmetric shape with oscillating abundances like that of the Ti zoning, though there is not a direct correlation. The chondrite-normalized signatures for each of the analysis points parallel one another, with minimal HREE variation (Fig. 8c).

Summarizing the observations, as displayed by these representative samples, major and trace element (including the transition metals) zoning is prominent in the lower grade garnet and diminishes at higher grades. The HREEs are more enriched than the LREEs and are most enriched in the garnet cores, decreasing outward, but contain inflections in the lower grade garnet. The HREE/LREE decreases significantly from core to rim, which is

also evident from a different perspective as higher variation in the HREE signatures on chondrite-normalized REE plots of individual analysis points. The lower-sillimanite-zone garnet has very little major or trace element zoning.

Discussion

Compositional zoning of major and trace elements in garnet is typically considered the result of one or more of the following: (1) elemental fractionation during mineral growth (e.g., Hollister 1966; Cygan and Lasaga 1982); (2) slow reequilibration of cations by intracrystalline (volume) diffusion (e.g., Anderson and Buckley 1973); (3) limitations at the mineral-matrix interface, such as limited intergranular diffusion of cations (e.g., Carlson 1989); (4) interaction with a metasomatic fluid (e.g., Hickmott et al. 1987; Young and Rumble 1993; Chamberlain and Conrad 1993; Erambert and Austrheim 1993; Jamtveit et al. 1993; Jamtveit and Hervig 1994); (5) the breakdown or growth of trace element–rich minerals (Hickmott and Spear 1992); or (6) changes in the garnet-mineral matrix partition coefficients because of changes in temperature, pressure, garnet composition, or the number of mineral phases in the assemblage or their proportions. These processes fall into two categories, those that occur during crystal growth and those that modify crystal chemistry after crystal growth. The majority of the processes occur during crystal growth. Diffusional reequilibration is the only primary postgrowth process that leads to zoning in minerals. In an extreme case, compositional zoning can arise in garnet after it has crystallized with a homogeneous composition that is out of equilibrium with the matrix. Because a chemical gradient exists between the garnet and the surrounding matrix, often biotite-rich, volume diffusion acts to reequilibrate the garnet composition with the matrix (e.g., Tracy et al. 1976). Diffusion occurs as long as the temperature remains sufficiently high (e.g., Lasaga 1983).

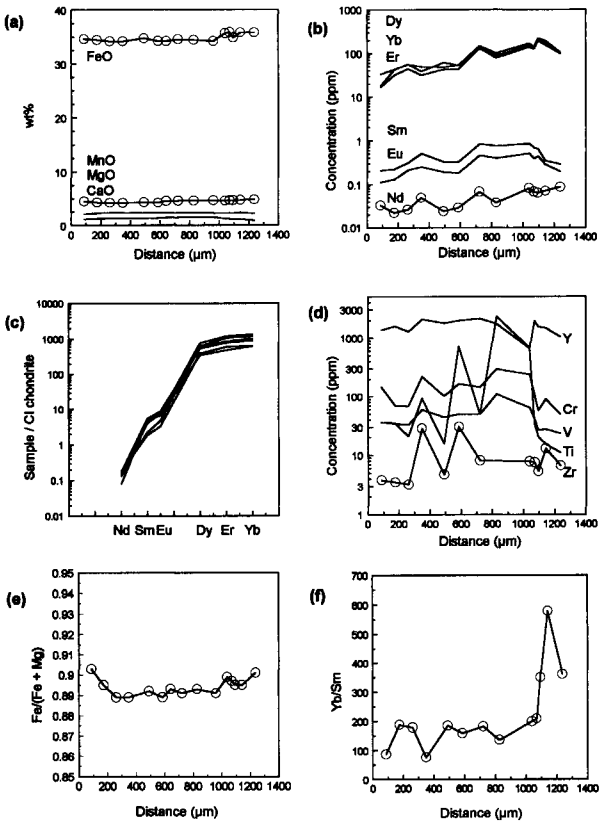

Figure 8. Rim-to-rim elemental zonation of lower-sillimanite-zone (SIZ) garnet (sample 1). Open circles mark positions of SIMS analyses and are the same for each element. (**a**) Rather homogeneous, major element zonation profile determined by EMP at the same positions as the SIMS analyses. (**b**) Irregular and asymmetric REE zonation profile. (**c**) Chondrite-normalized REE plot of individual SIMS analysis points. (**d**) Irregular and variable transition element zonation profile. (**e**) Fe/(Fe + Mg) profile. (**f**) HREE/LREE profile.

Effect of volume diffusion on zonation in Black Hills garnet

Volume diffusion is unlikely to have played a significant role in forming or modifying the compositional zoning in the Black Hills garnet. No changes in major element zoning occur near the garnet rims that are in contact with biotite (e.g., Fig. 2), staurolite, or aluminosilicate, which would suggest diffusional readjustment (cf. Tracy 1982; Lasaga 1983; Spear et al. 1991). If volume diffusion were a significant process it should have smoothed the inflections in the trace element concentrations, leading to flatter profiles, unless the diffusion coefficients are significantly smaller for the trace elements than for the major elements. Schwandt et al. (1995, 1996) experimentally determined that Ca self-diffusion in grossular is about one and one-half orders of magnitude slower than Mg self-diffusion in pyrope. Tracy et al. (1992) inferred from garnet from amphibolite-facies rocks that Ca diffusion was slower than diffusion of Mg, Fe, and Mn. This demonstrates that mineral composition is an important parameter when considering diffusion and that larger cations tend to diffuse more slowly than smaller cations. Because the trivalent rare earth elements are larger than the divalent cations they substitute for (e.g., Shannon and Prewitt 1969), their zoning profiles are unlikely to have been affected by diffusional homogenization. However, because the rare earth elements are trivalent, there is a charge-balance problem that may be accommodated by site vacancies, effectively enhancing the defect structure. This could increase the rate of diffusion of the REEs relative to that of the divalent cations. Harrison and Wood (1980) measured Sm diffusion coefficients for pyrope and grossular garnet at temperatures above 1200 °C. Extrapolation of their high-temperature experimental data down to metamorphic temperatures yields diffusion coefficients that are a few orders of magnitude faster than the coefficients experimentally determined for major elements. However, caution in interpretation is advisable because

different diffusion mechanisms are likely to operate in each temperature range; therefore, it is unwise to rely on such extrapolations (e.g., Lasaga 1981). It is interesting, though, that the larger LREEs have fewer inflections in their zoning than the smaller HREEs in the GZ garnet.

From the equation $d = (4Dt)^{1/2}$, where d is distance, D is the diffusion coefficient, and t is time, one can get a qualitative feel for the distances of diffusion over a given period at a given temperature. Using the Mg self-diffusion coefficients of Schwandt et al. (1995) and a temperature of 600 °C, maximum diffusion distances range from 0.6 μm for 10^5 yr to 5.7 μm for 10^7 yr. Using the Ca self-diffusion data of Schwandt et al. (1996), the maximum diffusion distances are even smaller. Therefore, even with long periods of elevated temperature the distance at which diffusional reequilibration may have taken place is smaller than the observed zoning.

In addition, profiles of the transition metals contain significant concentration inflections (Figs. 4d, 5d, 6d, 7d, and 8d), which are real but do not correlate with the major element zoning. As a representative example, comparison of the Ti profile of sample 23 (Fig. 4d) and the digital WDS Ti map of this sample (Fig. 2) revealed that Ti zonation is actually irregular. The lower-sillimanite-grade garnet (e.g., Fig. 8) has larger variations in transition-metal zoning. Given that this garnet was subject to the highest grade conditions, where diffusion would have been the most significant, the existence of transition-metal zoning is an argument against volume diffusion as an important mechanism for the development of trace element zoning in the XMS garnet. Also, there is insufficient experimental or theoretical evidence to suggest that the rates of diffusion of transition-metal cations through the garnet structure are different from those of the major element cations.

Effect of growth on processes of zonation

Although zonation of the major and trace elements is inconsistent with formation by reequilibration-related volume diffusion, it is consistent with formation by one or more growth processes. Profiles of the Fe/(Fe + Mg) ratios in the garnet-zone garnet are core enriched and decrease toward the rims (Figs. 4e and 5e). This has been suggested to be an indication of garnet growth dictated by a given garnet-producing reaction and increasing temperature (Spear et al. 1991; Spear 1993). Interestingly, the sample from the garnet zone closest to the staurolite isograd (Fig. 5e) and the garnet crystals in the staurolite and lower sillimanite zones (Figs. 6e, 7e, and 8e) have inflections in Fe/(Fe + Mg), which start from 50 to 200 μm from the garnet rims and could indicate a change in the garnet-forming reaction. However, in general, the Fe/(Fe + Mg) profiles of all the crystals of garnet are somewhat variable, which suggests the profiles are the result of a growth mechanism without subsequent reequilibration. This is consistent with garnet growth in the XMS unit during heating and mild decompression (e.g., Helms and Labotka 1991). Thus, the Fe/(Fe + Mg) profiles, the trace element profiles, and the euhedral garnet boundaries without reaction rims suggest that the zoning is the result of growth mechanisms.

Major element zonation, especially Mn and Fe zonation, is most consistent with a fractionation process during garnet growth. As the Fe/(Fe + Mg) profiles for the garnet-zone and some of the staurolite-zone garnet gently decrease from core to rim and indicate no drastic changes in temperature or pressure conditions (Spear et al. 1991; Spear 1993), the bell-shaped Mn profiles result from depletion of the matrix Mn by garnet that formed early, leaving less Mn for later garnet as the modal amount of garnet increased (Hollister 1966; Loomis 1975, 1976; Trzcienski 1977; Woodsworth 1977; Cygan and Lasaga 1982; Spear et al. 1991). However, modeling of the Mn profiles using the Rayleigh Fractionation approach of Hollister (1966) and Cygan and Lasaga (1982) indicates that the partitioning of Mn changed during garnet growth. Use of a constant partition coefficient for Mn causes the model zonation to begin the core-to-rim decrease much earlier than the measured profiles (Schwandt 1991). The measured Mn profiles of the XMS garnet (Figs. 4a and 5a) have high concentrations across much of the cores, looking more like the profiles of inverted bowls than bells, and cannot be modeled with a constant distribution coefficient. Also, smaller garnet grains in the same garnet-zone matrix contain similar, though less pronounced, zoning as adjacent larger garnet grains (Fig. 2).

Alternatively, Carlson (1989) suggested that the development of Mn zoning can be explained by limited intergranular diffusion of Mn through the matrix. Garnet growth is initiated and subsequently depletes the surrounding matrix of Mn. Carlson (1989) suggested that this process produces clusters of garnet within the matrix, which are observed in the garnet zone. This model implies that the diffusion rates of the various cations through the matrix are quite different. In this case, the intergranular diffusion of Mn would be significantly slower than that of Mg, Fe, and Ca. The major element profiles (Figs. 4–8) do not provide sufficient evidence to distinguish between fractionation and inadequate intergranular diffusion.

In contrast to the major element zonation, which contains no concentration inflections, the concentration inflections present in the trace element zonation (Figs. 4–8) are not directly explainable by a simple fractionation process. The variations in trace element concentrations from core to rim suggest that additional processes were operating during garnet growth. Although the concentrations of most of the trace elements decrease toward the garnet rims, suggesting the operation of a fractionation process, the concentration inflections of several elements suggest (1) variations in element concentration at the garnet-matrix interface because of changes in intergranular diffusion-related limitations, (2) reactions involving other mineral phases that resulted in fluctuation of the garnet-matrix bulk distribution coefficient during garnet growth, or (3) influx of metasomatic fluids.

The variable and asymmetric inflections in the zoning of transition metals (Cr, Ti, V, and Zr; Figs. 4–8), especially in garnet from the staurolite and lower sillimanite zones, provide additional clues about which mechanisms were important. The transition metals, especially Cr and V, have high crystal-field stabilization energies, which cause them to be more stable in distorted crystal-structure sites and to be very resistant to substitution reactions that result in relative enrichment in remnant precursor minerals (Burns 1993). Given this, if mineral-in or mineral-out reactions that utilize the transition metals as principle or minor components had occurred during garnet growth, then the zonation of transition metals should be minimal and symmetric about the garnet cores and contain few concentration inflections. Cr and V zonation in the garnet and staurolite zones is symmetric and contains few inflections, but in the lower sillimanite zone the zonation is variable and asymmetric, perhaps as the result of staurolite and ilmenite breakdown.

Variations in Zr zonation can be explained by equilibrium growth of zircon during garnet growth. In GZ sample 23 (Fig. 4), Zr concentration is low, and without zonation in the central portion of the garnet, but increases toward the garnet rims by more than a factor of ten, suggesting that zircon was no longer buffering Zr concentration. In the other samples, the Zr zonation profiles contain many concentration inflections, suggesting that Zr was not being consistently buffered by zircon even though it occurs in the matrix.

Alternatively, the lack of core-to-rim symmetry and the numerous inflections in the zonation suggest that the concentrations of transition metals did not remain everywhere constant at the growing garnet-matrix interface. This is best explained by limited and variable intergranular diffusion of the transition metals during garnet growth. Other alternative explanations such as changes in the mineral assemblage, which would affect the partitioning, are unlikely because the assemblage remains the same except for the occurrence of staurolite and andalusite or sillimanite. There is no clear correspondence between the zonation of transition metals in the garnet and the presence or proximity of staurolite or aluminosilicate. Limited or variable intergranular diffusion during garnet growth also accounts for the differences in zoning among garnet samples. For instance, the profiles of zonation of transition metals in the two garnet-zone samples (Figs. 4d and 5d) are rather different, as are those of the staurolite-zone samples (Figs. 6d and 7d). Such disparate variations are difficult to explain by the appearance and disappearance of other phases rich in trace elements, especially when there is little evidence for their presence at any point during the development of the XMS unit. In addition to variable intergranular diffusion and bulk partition coefficient changes resulting from changes in the matrix assemblage, the introduction of metasomatic fluids is an alternative explanation.

It is well documented that many trace element–rich pegmatites occur around the HPG (Duke et al. 1988; Shearer et al. 1992). Also, the bulk-rock chemistry of the XMS unit is enriched with large ion lithophile elements such as Cs and Rb (Schwandt 1991) by two times relative to the average crust, as determined by Taylor and McLennan (1981). Therefore, the increase in HREE concentrations about two-thirds of the distance from the core to the rim of the GZ garnet (Fig. 5) could be the result of the influx of a metasomatic fluid rich in HREEs (e.g., Hickmott et al. 1992) during garnet growth. Although it is possible that REE-rich metasomatic fluids interacted with the XMS unit of the Black Hills, the present evidence does not conclusively conclude that the trace element zoning inflections resulted from interaction with an REE-enriched metasomatic fluid.

Other possible causes of zonation

Although fractionation and variable intergranular diffusion processes may account for some aspects of the trace element zonation, they do not account for all aspects. Interestingly, the fact that the zoning profiles of the LREEs do not parallel the profiles of the HREEs in individual garnet grains (Figs. 4–7) suggests that the bulk garnet-matrix partition coefficients, particularly for the HREEs, changed during garnet growth. This is strongly supported by both the variability of the HREEs as depicted by the chondrite-normalized signatures and by the variable HREE/LREE (Yb/Sm) profiles across the garnet. The garnet cores are much more enriched with HREEs than the garnet rims. The LREE signatures for cores and rims have very similar chondrite-normalized signatures.

HREE partitioning may be more dependent on the major element composition of the garnet and only indirectly dependent on temperature and pressure. Specifically, garnet that contains high concentrations of Mn, and to a lesser extent Ca, in the core also has enhanced HREE content relative to LREE content in the core (Figs. 4–6). Garnet that is Fe rich has the same HREE/LREE from core to rim, as shown by the chondrite-normalized signatures (Fig. 8). Larger mole proportions of grossular and spessartine in the garnet structure enhance the compatibility of the light and heavy rare earth elements, respectively, as was previously observed by Schwandt et al. (1993). Larger major element cations in the eightfold-coordinated site of the garnet structure provide a more open structure that allows for more substitution of larger trace element cations (Novak and Gibbs 1971). Similar correlations of REE content with the Ca content have been observed in pyroxene (Shearer et al. 1989) and in pyroxene element-partitioning experiments (McKay et al. 1986; McKay 1989). Therefore, trace element partitioning is influenced by garnet composition and in this case affects the HREE/LREE in Mn-rich garnet cores. In Ca-rich rocks, Hickmott and Spear (1992) observed both positive and negative correlations of REE content with grossular component, depending on the bulk-rock composition and the presence of trace element–rich phases like clinozoisite.

In the present work, the strong core-to-rim decreases

in HREE/LREE correlate best with decreasing Mn concentrations (Figs. 4–8). Some of the inflections in the rimward portions of the garnet (Figs. 4, 5, and 8) could be the result of the breakdown of HREE-bearing matrix phases (e.g., Hickmott and Shimizu 1990; Hickmott and Spear 1992), but the overall core-to-rim decreases in HREE and HREE/LREE are best explained by a decreasing, compositionally dependent, HREE partition coefficient. The Hickmott and Spear (1992) work demonstrates the dependence of trace element partitioning on bulk-rock composition and phase assemblage. The present work, using a homogenous bulk composition, demonstrates the importance of garnet composition, which is a function of temperature and pressure, on trace element partitioning.

Ideally, it would be preferable to measure the trace element compositions of all the assemblage minerals. However, ion microprobe standards are available for only a few minerals. As more standards are characterized, the ability to determine more about the partitioning of trace elements in metamorphic systems will increase. Although this investigation of the XMS unit does not uncover profound new mechanisms that led to its development, the study does suggest that major and trace element zoning formed by growth processes and that elemental mobility within the XMS unit was perhaps limited. Thus, while thousands of pegmatites occur in the schists surrounding the Harney Peak Granite, metasomatic fluid flow through the XMS does not appear to have been significant during garnet growth. This contrasts with recent research on zoned minerals by others (e.g., Erambert and Austrheim 1993; Jamtveit and Hervig 1994) that suggests greater influence of metasomatic fluids. More important, however, this study provides further groundwork for the incorporation of trace element analysis into the study of metamorphic petrogenesis.

Acknowledgments

This research was supported by the Institute for the Study of Mineral Deposits, South Dakota School of Mines and Technology, and the Institute of Meteoritics, University of New Mexico (UNM). Electron microprobe data were obtained at the Electron Microbeam Facility, UNM. The ion microprobe data were obtained at the Ion Microprobe Facility at Woods Hole Oceanographic Institute. We thank Nobu Shimizu for his help with the ion microprobe analyses. Helpful reviews by D. Hickmott, M. Williams, C.T. Foster, Jr., A. Koziol, and B. Dutrow improved this manuscript.

References cited

Anderson, D.E., and Buckley, G.R. (1973) Zoning in garnets: Diffusion models. Contributions to Mineralogy and Petrology, 40, 87–104.

Banno, S., and Matsui, Y. (1973) On the formulation of partition coefficients for trace element distribution between minerals and magma. Chemical Geology, 11, 1–15.

Bence, A.E., and Albee, A.L. (1968) Empirical correction factors for the electron microanalysis of silicates and oxides. Journal of Geology, 76, 382–403.

Burns, R.G. (1993) Mineralogical application of crystal field theory (2nd edition), 551 p. Cambridge University Press, Cambridge, U.K.

Carlson, W.D. (1989) The significance of intergranular diffusion to the mechanisms and kinetics of porphyroblast crystallization. Contributions to Mineralogy and Petrology, 103, 1–24.

Chamberlain, C.P., and Conrad, M.E. (1993) Oxygen-isotope zoning in garnet: A record of volatile transport. Geochimica et Cosmochimica Acta, 57, 2613–2629.

Colson, R.O., McKay, G.A., and Taylor, L.A. (1988) Temperature and compositional dependence of trace element partitioning: Olivine/melt and orthopyroxene/melt. Geochimica et Cosmochimica Acta, 52, 539–553.

Cygan, R.T., and Lasaga, A.C. (1982) Crystal growth and the formation of chemical zoning in garnets. Contributions to Mineralogy and Petrology, 79, 187–200.

DeWitt, E., Redden, J.A., Buscher, D., and Wilson, A.B. (1989) Geologic map of the Black Hills area, South Dakota and Wyoming. Department of the Interior, U.S. Geological Survey Map, I-1910.

Drake, M.J., and Weill, D.F. (1975) Partition of Sr, Ba, Ca, Y, Eu^{2+}, Eu^{3+}, and other REE between plagioclase feldspar and magmatic liquid: An experimental study. Geochimica et Cosmochimica Acta, 39, 689–712.

Duke, E.F., Redden, J.A., and Papike, J.J. (1988) Calamity Peak layered granite-pegmatite complex, Black Hills, South Dakota: Part 1. Structure and emplacement. Geological Society of America Bulletin, 100, 825–840.

Erambert, M., and Austrheim, H. (1993) The effect of fluid and deformation on zoning and inclusion patterns in poly-metamorphic garnets. Contributions to Mineralogy and Petrology, 115, 204–214.

Ferry, J.M., and Spear, F.S. (1978) Experimental calibration of the partitioning of Fe and Mg between biotite and garnet. Contributions to Mineralogy and Petrology, 66, 113–117.

Ford, C.E., Russell, D.G., Craven, J.A., and Fisk, M.R. (1983) Olivine-liquid equilibria: Temperature, pressure and compositional dependence of the crystal/liquid cation partition coefficients for Mg, Fe^{2+}, Ca and Mn. Journal of Petrology, 24, 256–265.

Goldschmidt, V.M. (1937) The principles of distribution of chemical elements in minerals and rocks. Journal of the Chemical Society, 655–672.

Hanson, G.N. (1978) Rare earth elements in petrogenetic studies of igneous systems. Annual Reviews of Earth and Planetary Sciences, 8, 371–406.

Harrison, W.J., and Wood, B.J. (1980) An experimental investigation of the partitioning of REE between garnet and liquid with reference to the role of defect equilibria. Contributions to Mineralogy and Petrology, 72, 145–155.

Helms, T.S., and Labotka, T.C. (1991) Petrogenesis of Early Proterozoic pelitic schists of the Southern Black Hills, South Dakota: Constraints on regional low-pressure metamorphism. Geological Society of America Bulletin, 103, 1324–1334.

Hickmott, D.D., Shimizu, N., Spear, F.S., and Selverstone, J. (1987) Trace-element zoning in a metamorphic garnet. Geology, 15, 573–576.

Hickmott, D., and Shimizu, N. (1990) Trace element zoning in garnet from the Kwoiek area, British Columbia: Disequilibrium partitioning during garnet growth? Contributions to Mineralogy and Petrology, 105, 619–630.

Hickmott, D.D., Sorensen, S.S., and Rogers, P.S.Z. (1992) Metasomatism in a subduction complex: Constraints from microanalysis of trace elements in minerals from garnet amphibolite from the Catalina Schist. Geology, 20, 347–350.

Hickmott, D., and Spear, F.S. (1992) Major- and trace-element zoning in garnets from calcareous pelites in the NW Shelburne Falls Quadrangle, Massachusetts: Garnet growth histories in retrograded rocks. Journal of Petrology, 33, 965–1005.

Hollister, L.S. (1966) Garnet zoning: An interpretation based on the Rayleigh fractionation model. Science, 154, 1647–1651.

Jamtveit, B., Wogelius, R.A., and Fraser, D.G. (1993) Zonation patterns of skarn garnets: Records of hydrothermal system evolution. Geology, 21, 113–116.

Jamtveit, B., and Hervig, R.L. (1994) Constraints on transport and kinetics in hydrothermal systems from zoned garnet crystals. Science, 263, 505–508.

Kohn, M.J., Valley, J.W., Elsenheimer, D., and Spicuzza, M.J. (1993) O isotope zoning in garnet and staurolite: Evidence for closed-system mineral growth during regional metamorphism. American Mineralogist, 78, 988–1001.

Lasaga, A.C. (1981) The atomistic basis of kinetics: Defects in minerals. In Mineralogical Society of America Reviews in Mineralogy, 8, 261–320.

——— (1983) Geospeedometry: An extension of geothermometry. In S.K. Saxena, Ed., Kinetics and equilibrium in mineral reactions, p. 81–114. Springer-Verlag, New York.

Loomis, T.P. (1975) Reaction of zoning of garnet. Contributions to Mineralogy and Petrology, 52, 285–305.

——— (1976) Compositional zoning of crystals: A record of growth and reaction history. In S.K. Saxena, Ed., Kinetics and equilibrium in mineral reactions, p. 1–60. Springer-Verlag, New York.

McKay, G.A. (1989) Partitioning of rare earth elements between major silicate minerals and basaltic melts. In Mineralogical Society of America Reviews in Mineralogy, 21, 45–78.

McKay, G., Wagstaff, J., and Yang, S.R. (1986) Clinopyroxene REE distribution coefficients for shergottites: The REE content of the Shergotty melt. Geochimica et Cosmochimica Acta, 50, 927–937.

Navrotsky, A. (1978) Thermodynamics of element partitioning: (1) Systematics of transition metals in crystalline and molten silicates and (2) Defect chemistry and the "Henry's Law problem." Geochimica et Cosmochimica Acta, 42, 887–902.

Newton, R.C., and Haselton, H.T. (1981) Thermodynamics of the garnet-plagioclase-Al_2SiO_5-quartz geobarometer. In R.C. Newton, A. Navrotsky, and B.J. Wood, Eds., Thermodynamics of minerals and melts, p. 131–147. Springer-Verlag, New York.

Norton, J.J., and Redden, J.A. (1990) Relations of zoned pegmatites to other pegmatites, granite, and metamorphic rocks in the southern Black Hills, South Dakota. American Mineralogist, 75, 631–655.

Novak, G.A., and Gibbs, G.V. (1971) The crystal chemistry of the silicate garnets. American Mineralogist, 56, 791–825.

Ratte, J.C. (1986) Geologic map of the Medicine Mountain quadrangle, Pennington County, South Dakota. U.S. Geological Survey Miscellaneous Geologic Map I-1654, scale 1:24000.

Ratte, J.C., and Wayland, R.G. (1969) Geology of the Hill City quadrangle, Pennington County, South Dakota: A preliminary report. U.S. Geological Survey Bulletin, 1271-B, 1–14.

Redden, J.A. (1963) Geology and pegmatites of the Fourmile quadrangle, Black Hills, South Dakota. U.S. Geological Survey Professional Paper, 297-D, 199–291.

——— (1968) Geology of the Berne Quadrangle Black Hills South Dakota. U.S. Geological Survey Professional Paper, 297-F, 343–408.

Redden, J.A., and Norton, J.J. (1975) Precambrian geology of the Black Hills. In U.S. Congress, Senate Committee on Interior and Insular Affairs, Mineral and water resources of South Dakota: United States 94th Congress, 1st session, 21–28.

Redden, J.A., Norton, J.J., and McLaughlin, R.J. (1982) Geology of the Harney Peak Granite, Black Hills, South Dakota. U.S. Geological Survey Open File Report, 82-481, 1–18.

Redden, J.A., Peterman, Z.E., Zartman, R.E., and DeWitt, E. (1990) U-Th-Pb geochronology and preliminary interpretation of Precambrian tectonic events in the Black Hills, South Dakota. In Geological Association of Canada Special Paper, 37, 229–251.

Riley, G.H. (1970) Isotopic discrepancies in zoned pegmatite, Black Hills, South Dakota. Geochimica et Cosmochimica Acta, 34, 713–725.

Schwandt, C.S. (1991) Intra- and intercrystalline behavior of trace elements during metamorphism: A SIMS study of garnets. Ph.D. dissertation, South Dakota School of Mines and Technology, Rapid City, South Dakota.

Schwandt, C.S., Papike, J.J., Shearer, C.K., and Brearley, A.J. (1993) Garnetites associated with the Broken Hill Pb-Zn-Ag orebodies, Australia: An investigation of REE chemistry of garnet by secondary ion mass spectrometry. Canadian Mineralogist, 31, 371–379.

Schwandt, C.S., Cygan, R.T., and Westrich, H.R. (1995) Mg self-diffusion in pyrope garnet. American Mineralogist, 80, 483–490.

——— (1996) Ca self-diffusion in grossular garnet. American Mineralogist, 81, 448–451.

Shannon, R.D., and Prewitt, C.T. (1969) Effective ionic radii in oxides and fluorides. Acta Crystallographie, 925–946.

Shearer, C.K., Papike, J.J., Simon, S.B., Galbreath, K.G., and Shimizu, N. (1989) An ion microprobe study of the intra-crystalline behavior of REE and selected trace elements in pyroxene from mare basalts with different cooling histories. Geochimica et Cosmochimica Acta, 53, 1041–1054.

Shearer, C.K., Papike, J.J., and Jolliff, B.L. (1992) Petrogenetic links among granites and pegmatites in the Harney Peak rare-element granite-pegmatite system, Black Hills, South Dakota. Canadian Mineralogist, 30, 785–809.

Shimizu, N., and Hart, S.R. (1982) Applications of the ion microprobe to geochemistry and cosmochemistry. Annual Reviews of Earth and Planetary Sciences, 10, 483–526.

Spear, F.S. (1993) Metamorphic phase equilibria and pressure-temperature-time paths, 799 p. Mineralogical Society of America, Washington, DC.

Spear, F.S., Kohn, M.J., Florence, F.P., and Menard, T. (1991) A model for garnet and plagioclase growth in pelitic schists: implications for thermobarometry and *P-T* path determinations. Journal of Metamorphic Geology, 8, 683–696.

Taylor, S.R., and McLennan, S.M. (1981) The composition and evolution of the continental crust: Rare earth element evidence from sedimentary rocks. Philosophical Transactions of the Royal Society of London, A301, 381–399.

Terry, M.P., and Friberg, L.M. (1990) Pressure-temperature-time path related to the thermotectonic evolution of an Early Proterozoic metamorphic terrane, Black Hills, South Dakota. Geology, 18, 786–789.

Tracy, R.J. (1982) Compositional zoning and inclusions in metamorphic minerals. In Mineralogical Society of America Reviews in Mineralogy, 10, 355–397.

Tracy, R.J., Robinson, P., and Thompson, A.B. (1976) Garnet composition and zoning in the determination of temperature and pressure of metamorphism, Central Massachusetts. American Mineralogist, 61, 762–775.

Tracy, R.J., Miller, S.J., Solberg, T.N., and Waldron, K.A. (1992) Documentation of diffusional modification of garnet growth zoning in amphibolite facies garnets. Geological Society of America Abstracts with Programs, 24, A219.

Trzcienski, W.E., Jr. (1977) Garnet zoning: Product of continuous reaction. Canadian Mineralogist, 15, 250–256.

Walker, R.J., Hanson, G.N., Papike, J.J., and O'Neil, J.R. (1986) Nd, O, and Sr isotopic constraints on the origin of Precambrian rocks, southern Black Hills, South Dakota. Geochimica et Cosmochimica Acta, 50, 2833–2846.

Woodsworth, G.J. (1977) Homogenization of zoned garnets from pelitic schists. Canadian Mineralogist, 15, 230–242.

Young, E.D., and Rumble, D., III (1993) The origin of correlated variations in in-situ $^{18}O/^{16}O$ and elemental concentrations in metamorphic garnet from southeastern Vermont, USA. Geochimica et Cosmochimica Acta, 57, 2585–2597.

MANUSCRIPT RECEIVED JUNE 5, 1995
MANUSCRIPT ACCEPTED MAY 10, 1996

APPENDIX TABLE 1. Garnet compositions: major element oxide (wt%) by EMP and trace elements (ppm) by SIMS

	Garnet-zone sample 23 SIMS traverse points								Garnet-zone sample 27	
SiO_2	37.38	37.60	36.83	37.78	37.47	38.77	37.73	39.26	37.25	37.42
Al_2O_3	22.26	22.00	21.98	21.44	21.32	21.32	21.53	22.04	20.89	20.99
MgO	2.44	2.07	1.73	1.41	1.46	1.69	2.06	2.38	2.41	2.46
FeO	34.79	32.53	28.91	26.33	26.22	28.14	31.63	34.66	35.37	34.15
MnO	4.57	7.59	9.98	13.94	13.95	11.67	8.55	5.13	4.02	4.75
CaO	1.09	1.30	1.96	2.76	2.07	2.36	1.25	1.18	1.06	1.01
TiO_2	0.01	0.00	0.03	0.07	0.16	0.18	0.00	0.02	0.03	0.02
Total	102.53	103.09	101.41	103.73	102.65	104.12	102.75	104.66	101.02	100.80
Distance (μm)	58	108	158	275	442	583	708	758	17	33
La	0.009		0.012			0.126	0.005			
Ce	0.007		0.035							
Nd	0.100	0.123	0.158	0.275	0.590	1.802	0.200	0.188	0.232	
Sm	1.510	1.350	2.101	1.685	2.375	7.950	1.541	2.115	2.048	2.475
Eu	0.785	0.736	1.588	1.452	2.126	8.127	1.311	0.983	1.207	1.456
Dy	23.421	45.742	155.309	67.853	132.525	172.476	78.753	17.121	31.002	48.937
Er	6.456	14.297	90.018	52.488	167.476	106.177	23.864	4.561	7.250	12.195
Yb	9.422	18.341	99.192	46.652	243.692	93.845	25.686	7.515	10.670	16.346
Ti	82.6	125.3	315.3	1037.8	326.9	1096.9	134.1	115.8	76.9	105.3
V	23.5	31.3	44.8	89.5	16.6	74.7	40.8	36.0	78.0	98.7
Cr	127.2	162.0	181.6	241.2		238.6	181.1	158.8	172.3	197.6
Y	42.0	392.2	914.5	672.2	322.7	346.4	477.6	67.3	74.7	213.6
Zr	27.0	2.7	5.5		8.7		4.5	79.0	7.7	6.9
	Garnet-zone sample 27									
SiO_2	36.75	36.75	37.10	37.16	36.61	37.70	37.10	37.38	37.45	37.88
Al_2O_3	20.61	20.46	20.45	20.48	20.57	20.36	20.52	20.99	20.83	20.92
MgO	2.32	2.09	1.80	1.53	1.20	1.36	1.87	2.06	2.33	2.59
FeO	32.69	30.77	29.41	27.04	24.53	26.43	29.45	30.80	33.10	34.45
MnO	6.33	7.35	8.79	10.93	13.50	12.85	9.21	8.58	6.49	4.35
CaO	1.52	2.32	2.46	2.43	2.58	2.59	2.11	1.47	1.16	1.08
TiO_2	0.02	0.04	0.06	0.08	0.12	0.15	0.06	0.05	0.01	0.03
Total	100.24	99.77	100.08	99.64	99.11	101.45	100.32	101.34	101.37	101.32
Distance (μm)	61	95	122		267	361	417		464	489
La				156				445		
Ce						0.432				
Nd	0.101			0.834		1.401	0.779			
Sm	1.252	4.697	3.370	3.982	8.707	9.612	6.591	1.828	1.351	2.867
Eu	1.650	3.808	2.566	3.695	5.246	5.207	5.629	1.784	0.575	1.383
Dy	176.495	265.995	122.647	91.163	467.906	562.814	228.404	264.342	36.460	33.690
Er	78.993	108.555	74.014	42.837	380.994	471.591	143.097	275.610	14.183	4.697
Yb	65.247	85.037	70.383	34.567	353.138	410.458	126.288	236.636	15.295	6.576
Ti	117.2	502.0	1150.0	44625.9	29722.3	4849.8	882.2	251.0	64.2	150.9
V	86.0	109.7	196.9	741.5	709.7	465.5	282.7	154.1	80.2	145.2
Cr	243.2	79.4	360.9	724.3	765.7	651.8	348.2	299.2	344.4	259.8
Y	1510.1	610.2	606.5	341.2	3531.1	1315.3	1187.4	960.6	401.0	94.6
Zr	4.3	6.1	6.1	21.1	1185.5	261.6	97.0	13.4	6.5	19.7
	Staurolite-zone sample 16									
SiO_2	37.29	37.56	36.43	36.99	37.15	36.53	36.56	37.15	37.28	36.31
Al_2O_3	20.72	20.85	20.43	20.02	20.2	20.41	20.12	20.58	20.27	20.27
MgO	3.04	3.26	3.04	2.14	2.36	2.46	2.78	3.25	3.18	3.39
FeO	25.06	24.96	23.23	19.9	19.88	20.48	21.35	24.03	24.1	24.62
MnO	12.58	12.64	13.7	15.71	15	14.86	13.33	13.38	12.55	12.31
CaO	1.32	1.83	2.33	4.2	3.5	3.38	3.34	1.48	2.31	2.3
TiO_2	0.02	0.03	0.07	0.12	0.08	0.08	0.12	0.07	0.1	0.08
Total	100.01	101.13	99.24	99.08	98.16	98.2	97.59	99.94	99.79	99.27
Distance (μm)	5	20	80	165	260	330	430	560	640	670
La					38.673	64.256	11.980			
Ce					76.980	133.020	37.025			
Nd	0.353	0.360	0.145	0.580	24.706	47.386	20.671	0.501	0.305	0.327
Sm	0.437	1.983	1.024	1.217	5.992	11.336	3.117	0.812	1.420	1.016
Eu	0.745	1.264	0.765	0.862	1.144	1.649	0.702	0.347	0.890	0.805
Dy	128.855	163.790	79.936	196.915	1000.000	701.000	593.600	305.236	162.536	67.472
Er	99.588	107.624	53.961	212.145	2602.000	3228.000	2651.000	1099.000	171.017	41.960
Yb	70.256	99.218	52.489	199.703	2413.000	4723.000	4141.000	1093.000	188.639	41.931
Ti	2777.0	99.3	479.4	956.1	734.9	692.4	592.2	475.9	812.7	467.1
V	113.2	33.4	71.3	77.1	82.4	77.1	74.3	77.1	72.9	67.2
Cr	165.4	121.2	143.7	139.1	152.4	132.4	82.1	117.8	121.0	137.8
Y	474.5	688.0	217.6	1225.3	9493.1	8710.2	6424.9	4247.9	1099.5	227.5
Zr	25.7	83.9	15.8	293.6	540.5	176.9	41.5	31.0	5.6	29.4

APPENDIX TABLE 1.—*Continued*

	Staurolite-zone sample 16		Staurolite-zone sample 40							
SiO_2	36.8	36.68	36.87	36.55	37.08	37.07	37.54	36.80	36.35	36.84
Al_2O_3	20.32	21.02	20.79	20.54	20.90	20.84	20.84	20.40	20.73	20.62
MgO	3.35	3.19	2.17	2.44	2.37	2.23	2.22	2.21	2.21	2.19
FeO	24.49	24.78	34.82	33.85	33.34	33.42	33.10	33.22	32.63	32.05
MnO	12.09	12.54	3.62	3.89	4.13	4.96	5.12	5.09	4.96	4.91
CaO	2.36	1.28	0.99	1.29	1.48	1.66	1.55	1.64	1.75	1.70
TiO_2	0.13	0.01	0.00	0.00	0.00	0.00	0.00	0.01	0.00	0.00
Total	99.55	99.5	99.26	98.56	99.30	100.17	100.37	99.37	98.63	98.32
Distance (μm)	700	750	57	114	157	271	357	471	586	671
La			4.857							
Ce			8.238							
Nd	0.204	0.083		1.966	0.262	0.175				0.142
Sm	1.497	0.572		0.498	0.733	0.575	0.512	0.589		0.494
Eu	1.079	0.555			0.549	0.474	0.350	0.286	0.201	0.312
Dy	51.672	220.885	6.611	0.281	19.755	45.980	55.932	52.437	37.694	63.904
Er	29.128	223.594	1.599	0.188	4.544	17.738	42.025	38.369	31.747	50.817
Yb	29.566	203.152	1.645		5.224	10.642	31.104	29.976	25.608	38.917
Ti		102.7	115.1	117.8	189.6	201.1	154.4	104.7	150.7	173.9
V	66.5	26.2	38.3	50.4	61.4	70.0	58.7	36.3	57.3	63.0
Cr	133.3	103.7	110.7	134.7	130.1	136.4	139.0	86.9	121.9	139.7
Y	126.5	708.6	95.9	220.2	332.3	1844.9	2277.5	874.3	2251.0	2415.6
Zr		5.6	137.3	15.5	13.1	25.1	19.7	8.1	8.3	10.1

	Staurolite zone sample 40					Lower-sillimanite-zone sample 1			
SiO_2	36.82	36.85	36.92	36.86	36.52	37.32	37.07	36.52	37.39
Al_2O_3	20.64	20.51	20.96	20.60	20.97	21.96	21.47	21.44	21.54
MgO	2.23	2.33	2.32	2.38	2.20	2.09	2.27	2.39	2.4
FeO	33.00	33.61	34.75	34.85	34.69	34.63	34.46	34.2	34.2
MnO	4.59	4.29	3.62	3.36	3.28	4.5	4.32	4.25	4.22
CaO	1.74	1.75	1.66	1.55	1.29	1.16	1.25	1.34	1.3
TiO_2	0.00	0.00	0.00	0.00	0.00	0.05	0.06	0.01	0
Total	99.02	99.35	100.23	99.61	98.94	101.72	100.88	100.15	101.15
Distance (μm)	814	914	1057	1114	1157	87			349
La								262	
Ce							175		
Nd	0.189		0.211			0.033	0.022	0.026	0.050
Sm	0.631	0.353	0.457	0.308	0.324	0.210	0.223	0.315	0.507
Eu	0.419	0.344	0.442		0.256	0.112	0.130	0.212	0.250
Dy	62.411	34.767	18.324	8.280	8.350	33.071	42.214	55.292	49.551
Er	37.431	15.768	4.261	2.641	2.783	16.989	31.594	43.617	31.466
Yb	24.461	10.268	3.990	3.872	3.931	18.182	41.930	56.442	38.571
Ti	157.2	111.1	169.3	163.8	122.6	36.3	35.2	21	93.4
V	61.2	66.8	69.1	40.1	38.5	35.9	34.6	32.6	59.5
Cr	138.3	146.3	165.4	103.3	110.9	146.1	71	68	220.2
Y	1712.3	1068.4	379.8	169.2	190.8	1372.4	1593.4	1284	2061.1
Zr	22.9	14.1	8.3	26.3	15.0	3.8	3.5	3.2	28.4

	Lower-sillimanite-zone sample 1								
SiO_2	36.92	37.54	37.44	37.44	38.05	37.21	37.97	37.94	37.78
Al_2O_3	21.57	21.61	21.76	22	21.82	21.86	21.49	21.77	21.6
MgO	2.35	2.41	2.37	2.32	2.25	2.32	2.29	2.36	2.21
FeO	34.74	34.25	34.54	34.44	35.66	35.84	34.84	35.78	35.79
MnO	4.33	4.26	4.63	4.63	4.64	4.72	4.69	4.76	4.84
CaO	1.33	1.36	1.48	1.52	1.27	1.17	1.16	1.13	0.9
TiO_2	0.08	0	0.02	0.05	0.01	0.01	0.01	0.02	0
Total	101.31	101.42	102.2	102.41	103.69	103.12	102.43	103.76	103.12
Distance (μm)	492	587	722	828	1039	1071	1095	1143	1238
La									
Ce									
Nd	0.024	0.029	0.068	0.039	0.082	0.068	0.064	0.071	0.088
Sm	0.331	0.331	0.825	0.751	0.851	0.676	0.638	0.348	0.291
Eu	0.192	0.183	0.461	0.398	0.515	0.385	0.439	0.286	0.196
Dy	47.772	54.357	138.000	88.824	149.864	138.925	195.858	158.248	98.148
Er	42.506	43.113	130.163	79.776	141.136	124.570	198.550	176.976	99.927
Yb	61.144	52.750	150.457	102.057	169.951	141.165	223.943	201.176	105.461
Ti	15.7	722.9	49.4	2301.9	684.2	34.6	20.3	15.3	10.9
V	44.2	50.1	49.3	108.9	64.4	42.1	26.6	27.5	23
Cr	102	164.2	144.9	296.5	236.6	109.9	57	89.8	49.6
Y	1795.9	1967.2	2114.7	1729.6	671.2	1954.9	1548.1	1471.1	1042.6
Zr	4.7	30.3	8.1		7.8	7.5	5.3	12.8	6.6